High-speed GaAs/AlGaAs optoelectronic devices for computer applications

by Ch. S. Harder
B. J. Van Zeghbroeck
M. P. Kesler
H. P. Meier
P. Vettiger
D. J. Webb
P. Wolf

We present an overview, mainly of work in our laboratory, of low-threshold GaAs/AlGaAs quantum-well laser diodes and GaAs metal–semiconductor–metal photodetectors—two optoelectronic devices which show good promise for use in computer-related communication. Present-day telecommunication device technology (based on InP materials) is not well suited to the requirements of optical data communication among and within computers because the computer environment is much more demanding. It imposes a higher ambient temperature on the devices, and requires denser packaging and smaller power dissipation per device, as well as a high degree of parallelism. The GaAs/AlGaAs device technology is ideally suited to this task because of the possibility of integration of arrays of high-speed, low-threshold laser diodes and high-speed photodetectors with high-performance electronic circuits.

©**Copyright** 1990 by International Business Machines Corporation. Copying in printed form for private use is permitted without payment of royalty provided that (1) each reproduction is done without alteration and (2) the *Journal* reference and IBM copyright notice are included on the first page. The title and abstract, but no other portions, of this paper may be copied or distributed royalty free without further permission by computer-based and other information-service systems. Permission to *republish* any other portion of this paper must be obtained from the Editor.

Introduction

As distances between computers—and their data transmission rates—increase, optical fibers become very attractive signal carriers. The optical data communication system envisaged would be similar to a long-haul telecommunication system in its use of lasers to generate optical signals, fibers to transport the signals over a distance of several kilometers, and photodiodes with which to convert the received optical signals into electrical signals. However, the technology requirements for optical data communication among and within computer systems are quite different from those of well-established optical telecommunication technology. For telecommunication, the data-rate–distance product of the fiber is of prime importance. For data communication, the most important aspect is the total time needed to send a data package from its source to its destination. In addition, the computer environment is very demanding: It imposes a higher ambient temperature on the optical

devices used and requires dense packaging and a small power dissipation per device, as well as a high degree of parallelism.

The possibility of integrating arrays of high-speed, low-threshold laser diodes and high-speed photodetectors with high-performance electronic circuits makes the GaAs technology very attractive for optical data communication. The GaAs/AlGaAs material system is ideally suited to this task because of its mature MESFET, laser diode, and photodetector technology. Highly integrated, very compact parallel links in this technology have already been successfully demonstrated [1].

In the first part of this paper, we discuss the high-speed characteristics of low-threshold GaAs/AlGaAs single-quantum-well (QW) laser diodes. Such diodes have the following advantages: low threshold current, high efficiency, low temperature sensitivity, and high speed at low power levels. We derive the equivalent electrical circuit of the QW laser diode and use this circuit to analyze the limits of high-speed small-signal modulation.

Second, we discuss the design, fabrication, and characterization of very high-speed GaAs metal–semiconductor–metal (MSM) photodiodes. They perform extremely well due to their low capacitance and the short transit time of their carriers. The relatively simple structure of the photodetectors allows them to be incorporated into high-speed GaAs integrated circuits. This makes it possible to reduce parasitic capacitances and inductances, which is crucial for obtaining sensitive and high-speed optoelectronic receivers.

High-speed quantum-well laser diodes

- *AlGaAs laser diodes*

In 1962 stimulated light emission in a forward-biased p–n junction was simultaneously observed by four independent groups [2]. This discovery of the laser diode triggered a flurry of activity directed mainly toward optical computation and optical data storage. Finally, after two decades of effort and several breakthroughs such as the development of the ternary $Al_xGa_{1-x}As$ single-crystal alloy and the quaternary $In_{1-x}Ga_xAs_yP_{1-y}$ single-crystal alloy, the laser diode has become a useful room-temperature device. In the past few years, the laser diode has started to dominate the laser field and has become the key element in an ever-increasing number of applications, particularly in optical-fiber communication (made possible by the development in 1966 of a means to produce low-loss silica fibers by Kao and Hockham [3]), optical data storage, and laser printers.

Laser diodes owe their success to their small size, high energy conversion efficiency, ease of use, and high reliability. Laser diodes are pumped by simply passing a current through them at current and voltage levels which are compatible with those of integrated circuits. The light emission can be modulated by switching pump current with switching times of less than 100 ps. Laser diodes can also be mass-produced with the same processing techniques used for electronic integrated circuits, and can be integrated with such circuits. This unique possibility has given birth to the field of monolithic optoelectronic circuits [4].

In the following sections, we first describe the structure of laser diodes, present their typical characteristics, and briefly discuss their fabrication. Then, we derive an electrical equivalent circuit for such a diode from rate equations for a QW laser diode. Such a circuit is necessary in order to understand fully the high-frequency behavior of a laser diode when it is driven by an electronic circuit. The upper limits to high-speed modulation are then discussed in detail. Finally, measurements of the small-signal modulation behavior and the large-signal pulse response of a single-QW laser diode are presented.

- *Quantum-well laser diodes*

During the past few years, the threshold current density of semiconductor laser diodes has been reduced gradually by making their active region thinner. In present laser diodes the carriers in the active region are confined by a potential well which is comparable in size to the de Broglie wavelength of the carriers. This causes quantum-mechanical effects to occur—thus the designation "quantum-well" laser diodes. The electrons as well as the holes in this active region must be described as a two-dimensional electron–hole plasma. The optical mode cannot be guided by such a thin active region, and an additional optical waveguide is provided to confine the light vertically to a single mode. The cross section of an illustrative laser diode is shown in **Figure 1**. The type of diode depicted was first proposed by Tsang [5] and is referred to as a graded-index separate-confinement heterostructure (GRIN-SCH) diode. The electrons and holes are confined to its central GaAs quantum well, which is surrounded by graded $Al_xGa_{1-x}As$ layers having a higher bandgap (x varies between 0.2 and 0.5). The optical mode is guided within this graded region because it has a higher index of refraction than the cladding layers ($x = 0.5$) on the top and bottom. The various additional quantum wells and superlattice (SL) serve to improve the crystal quality.

If a current is passed vertically through the device, light is emitted through the front and back facets. The holes are injected into the active quantum well through the p-type-doped top cladding layer, and the electrons are injected through the n-type-doped lower cladding. Although the ridge laser structure shown in Figure 1 provides good optical lateral mode control by means of a ridge which is embedded in polyimide, it does not

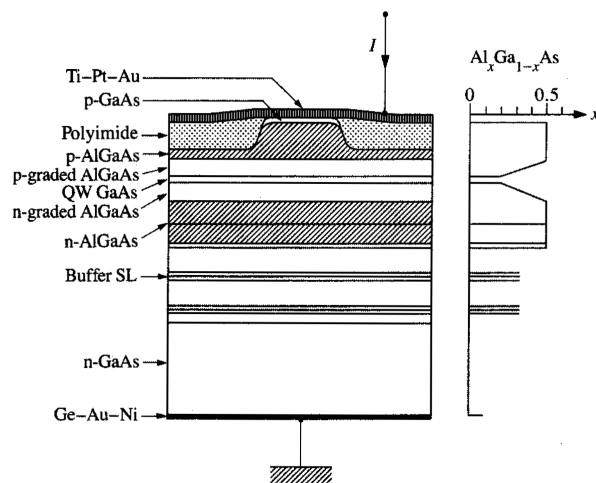

Figure 1

Cross section of a ridge GRIN-SCH single-quantum-well laser diode and associated relative concentration of aluminum.

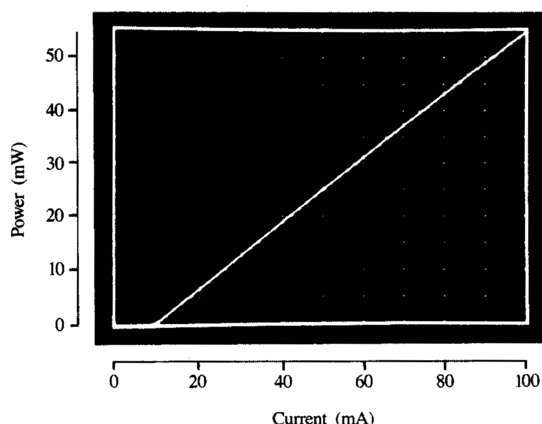

Figure 2

Light-current characteristic of the diode of Figure 1. Dimensions: 400 μm long, with a ridge 3 μm wide. The threshold current is 9 mA and the differential efficiency of the front facet is 0.6 mW/mA.

provide lateral confinement for the carriers and offers only a weak lateral confinement for the injected current. Its light output as a function of the drive current is shown in **Figure 2**. At low currents, it functions as an edge-emitting LED (light-emitting diode), and only a small fraction of the light (which is emitted isotropically) leaves the laser diode through the front facet. At threshold current, the round-trip gain in the cavity becomes unity and laser oscillation sets in. Above threshold current, all additional injected current is converted into photons through stimulated emission. Typical threshold currents for single-QW laser diodes range between 0.5 mA and 10 mA, and typical differential efficiencies of the front facet are between 0.6 mW/mA and 1.1 mW/mA.

Fabrication process

As described in [6], the various $Al_xGa_{1-x}As$ layers for the vertical carrier and photon confinement are first grown by molecular beam epitaxy on an n-doped, 2-inch-diameter GaAs substrate. A silicon-doped buffer layer (1 μm GaAs, $n = 1 \times 10^{18}$ cm^{-3}) is grown on the substrate, followed by the lower cladding layer (1.25 μm $Al_{0.5}Ga_{0.5}As$, $n = 5 \times 10^{17}$ cm^{-3}). The core of the laser consists of a linearly graded region (0.2 μm $Al_{1-x}Ga_xAs$, $n = 2 \times 10^{17}$ cm^{-3}), an undoped active region (7 nm GaAs), and a linearly graded region (0.2 μm $Al_{1-x}Ga_xAs$, $p = 2 \times 10^{17}$ cm^{-3}). The top cladding layer (1.25 μm $Al_{0.5}Ga_{0.5}As$, $p = 5 \times 10^{17}$ cm^{-3}) is followed by a heavily p-doped contact layer. The doping density of this top layer is high enough to permit formation of a good ohmic contact to a nonalloyed electrode consisting of titanium, platinum, and gold. Measured threshold current densities are as low as 120 A/cm^2, and waveguide losses are as low as $\alpha = 2$ cm^{-1}.

The processing of the laser structure is as follows: First, 5-μm-wide photoresist strips are patterned on the top side of the wafer to define the ridges. The ridge waveguide is formed by etching away 1.2 μm of the top layers with a wet etch at room temperature (H_2SO_4:H_2O_2:H_2O = 1:8:1000). Etching is stopped 0.2 μm above the graded index part of the cladding layer; this results in good lateral-mode confinement. Because of the under-etching, the ridge waveguide becomes 3–4 μm wide. After etching, the photoresist mask is removed, yielding the cross section shown in **Figure 3(a)**.

For a high-speed laser diode, the top contact should have only a small capacitance with regard to the substrate. This is achieved by embedding the ridge with a thick layer of a material having a low dielectric constant, and does not introduce excessive stress, which would adversely affect reliability. For this purpose, use is made of a polyimide [7] which is spin-coated onto the wafer in two stages. The total thickness of the polyimide at this point is about 2.5 μm; the top surface of the polyimide contains undulations which reflect the underlying ridge structure, but of a greatly reduced amplitude; i.e., the structure has been somewhat "planarized." A further

degree of planarization is achieved by spinning on a Shipley AZ 4210 photoresist layer to a total thickness (photoresist plus polyimide) of about 7.2 μm [**Figure 3(b)**]. The entire top surface of the composite is then etched using oxygen-reactive ion etching (RIE) to a depth sufficient to expose the tops of the ridges, to which self-aligned ohmic contacts are subsequently applied as illustrated in **Figure 3(c)**. To obtain ohmic contact to the n-type substrate, germanium, gold, and nickel are alloyed to the back of the GaAs wafer. Finally, the wafers are cleaved, the mirror facets are protected with a thin layer of Al_2O_3, and the laser diodes are then soldered (junction side up) onto a high-speed mount. Connections to their p-contacts are made by gold-wire bonding.

- *Small-signal equivalent circuit*

The laser diode is an optoelectronic device with electrical as well as optical characteristics [8]. The many applications of laser diodes, in particular those which involve high-frequency modulation or combined operation with electronic components and circuits, require an accurate representation of the electrical characteristics of the laser diode. In this section, we introduce rate equations which describe the QW laser diode and derive the associated equivalent electrical circuit.

Usually such rate equations are formulated for volumetric densities (cm^{-3}) of carriers and photons. In quantum wells, only the areal densities (cm^{-2}) of the carriers, and in single-mode waveguides only the areal density of the photons, are of significance. Therefore we have reformulated these rate equations in particles per unit area. We assume that the active region is undoped, that it consists of n identical quantum wells, and that the density of injected holes is equal to the density of injected electrons (quasi-neutrality). The voltage across the diode is designated as V, the pump current density as J, the photon density as S, and the electron density per quantum well as N. All densities are expressed in cm^{-2}. The rate equations can then be expressed as

$$\frac{dN}{dt} = \frac{J}{en} - R(N) - v_{gr}\Gamma G(N, S)S, \tag{1a}$$

$$\frac{dS}{dt} = -\frac{S}{\tau_S} + \beta R(N)n + v_{gr}\Gamma G(N, S)Sn, \tag{1b}$$

$$V(N) = \frac{E_g}{e} + V_T \ln[(e^{N/N_C} - 1)(e^{N/N_V} - 1)]. \tag{1c}$$

The symbols used in these equations and the typical values of the device and materials constants are listed in **Tables 1** and **2**. Equation (1a) states that the change of carrier density is equal to the pump rate less the spontaneous emission rate $R(N)$ less the stimulated emission rate. This stimulated emission rate is

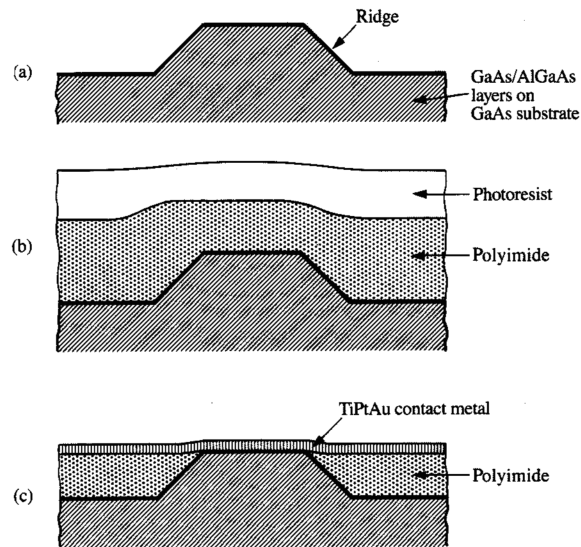

Figure 3

Cross sections illustrating ridge-embedding technique for fabricating the diode of Figure 1. First, the ridge waveguide is etched (a), then polyimide is applied to planarize the surface (b), and finally the ohmic contact is formed (c).

Table 1 AlGaAs material and device constants.

Electron charge:	$e = 1.60 \times 10^{-19}$ A-s
Planck's constant:	$h = 6.63 \times 10^{-34}$ W-s^2
Effective density of states of electrons:	$N_C \simeq 0.72 \times 10^{12}$ cm^{-2}
Effective density of states of holes:	$N_V \simeq 4.86 \times 10^{12}$ cm^{-2}
Bandgap of quantum well:	$E_g \simeq 1.46$ eV
Linear recombination constant:	$\tau \simeq 2 - 10 \times 10^{-9}$ s
Quadratic recombination constant:	$\bar{B} \simeq 5 \times 10^{-5}$ cm^2-s^{-1}
Differential lifetime:	$\tau_N \simeq 1 \times 10^{-9}$ s
Differential gain:	$\mathscr{G} \simeq 4 \times 10^{-10}$ cm
Differential gain saturation:	$\varepsilon \simeq 2 \times 10^{-9}$ cm
Group velocity:	$v_{gr} \simeq 0.75 \times 10^{10}$ cm-s^{-1}
Lasing photon energy:	$h\nu \simeq 1.46$ eV
Thermal voltage:	$V_T = 25.9 \times 10^{-3}$ V at $T = 300$ K

proportional to the optical confinement factor Γ and the gain $G(N, S)$ of an optical wave completely confined to one QW. The optical confinement factor Γ is equal to the overlap integral of the vertical photon density profile with one QW [9] and is typically $\Gamma \simeq 0.02$–0.04 (Γ is independent of the number n of quantum wells). In Equation (1b), the change of the density of photons in the waveguide is given by minus the loss of photons S/τ_S,

Table 2 Device variables.

Variable	Symbol (unit)
Current:	I (A)
Current density:	J (A-cm^{-2})
Voltage:	V (V)
Carrier density in one quantum well:	N (cm^{-2})
Spontaneous recombination rate in one quantum well:	$R(N)$ (cm^{-2}-s^{-1})
Optical gain of one quantum well:	$G(N)$ (cm^{-1})
Photon density:	S (cm^{-2})
Waveguide loss:	α (cm^{-1})
Spontaneous emission coupling constant:	β
Photon lifetime in cold cavity:	τ_S (s)
Optical confinement factor:	Γ
Number of QWs in laser diode:	n
Width of laser diode:	W (cm)
Length of laser diode:	L (cm)
Reflectivity of laser mirror:	R
Ideality factor:	m
Differential quantum efficiency (front mirror):	η
Damping factor:	γ (s^{-1})
Relaxation resonance:	ω_r (s^{-1})
Maximum 0-dB bandwidth:	$\omega_{0,\max}$ (s^{-1})

plus a small amount of spontaneous emission which is coupled into the lasing mode, plus the stimulated rate. The photon lifetime is $\tau_S = 1/\{v_{gr}[\alpha + 1/L \ln(1/R)]\}$ and the output power P through one facet is proportional to the photon density S inside the cavity, $P = Sh\nu/2v_{gr}W \ln(1/R)$. Equation (1c) relates the voltage across the laser diode (which is equal to the separation between the quasi-Fermi levels of the electrons and the holes) to the carrier density in the quantum wells. This relationship is given by a simple analytic expression as long as only one sub-band in the QW is populated.

We obtain the static solution of the set of rate equations (1) by setting the time derivatives to zero. We then assume that the coupling of the spontaneous emission into the lasing mode and the gain saturation are both very small ($\beta \simeq 0$, $\varepsilon \simeq 0$) and find from Equation (1b) that the gain G is approximately clamped to a threshold value G_0 which equals the cavity losses. The clamping of the gain in turn clamps the carrier density to the value N_0, and

$$G_0(N_0, S_0) \simeq \frac{1}{\tau_S}\frac{1}{n\Gamma v_{gr}}, \tag{2a}$$

$$S_0 \simeq \frac{J_0 - J_{th}}{e}\tau_S, \tag{2b}$$

$$J_{th} = eR_0 n, \tag{2c}$$

$$V_0 = \frac{E_g}{e} + V_T \ln[(e^{N_0/N_C} - 1)(e^{N_0/N_V} - 1)]. \tag{2d}$$

The subscript 0 indicates that these values are static values. Above the laser threshold, the gain, the carrier density, and the voltage do not change with drive current. The light output P_0 is linear with the current density J_0 above threshold, as follows from Equation (2b). This justifies carrying out a small-signal analysis of the rate equations in order to derive the electrical equivalent circuit. Accordingly, we introduce the following small-signal values: $J = J_0 + J_1(t)$, $N = N_0 + N_1(t)$, $S = S_0 + S_1(t)$, $P = P_0 + P_1(t)$, and $V = V_0 + V_1(t)$.

Assuming that bimolecular recombination processes dominate, and that low background doping is used, the spontaneous recombination rate is given by

$$R(N) = \frac{N}{\tau} + \bar{B}N^2. \tag{3a}$$

The constant $\bar{B}$ is the bimolecular recombination constant, and τ is the lifetime at low injected carrier densities. For the small-signal analysis, the recombination rate is linearized in carrier density, viz:

$$R(N) = R_0 + \frac{1}{\tau_N}N_1(t), \tag{3b}$$

with

$$\tau_N = \frac{1}{2\bar{B}N_0 + \frac{1}{\tau}}. \tag{3c}$$

The gain is linearized in carrier density and photon density,

$$G(N, S) = G_0 + \ell N_1(t) - \varepsilon S_1(t), \tag{4}$$

where ℓ is the differential gain constant.

Modal gain saturation ($\varepsilon > 0$) is caused by one or more of the following effects: spatial hole burning, dynamic carrier heating, and spectral hole burning.

We also linearize the voltage [Equation (1c)] as a function of carrier density, viz:

$$V_1(t) = \frac{mV_T}{N_0}N_1(t), \tag{5a}$$

with

$$m = \frac{\frac{N_0}{N_C}}{(1 - e^{-N_0/N_C})} + \frac{\frac{N_0}{N_V}}{(1 - e^{-N_0/N_V})}. \tag{5b}$$

Substituting the above-defined linear relations into the rate equations (1) and eliminating the carrier density N_1, we obtain the following set of differential equations describing the small-signal characteristics of the laser diode,

$$\frac{dV_1}{dt} = \frac{mV_T}{N_0}\frac{J_1}{en} - V_1\left(\frac{1}{\tau_N} + v_{gr}\Gamma\ell S_0\right) - \frac{mV_T}{N_0}S_1 v_{gr}\Gamma(G_0 - \varepsilon S_0), \tag{6a}$$

$$\frac{dS_1}{dt} = \frac{N_0}{mV_T} V_1\left(\frac{\beta}{\tau_N} + v_{gr}\Gamma\ell S_0\right)n$$

$$- S_1\left[\frac{1}{\tau_S} - v_{gr}\Gamma(G_0 - \varepsilon S_0)n\right]. \qquad (6b)$$

This set is identical to that which describes an electrical circuit consisting of a capacitor C, in parallel with a resistor R and a branch consisting of an inductor L with a damping resistor R_d. Such a circuit is shown in **Figure 4**, augmented with a parasitic bond-wire inductance L_B, a parasitic pad capacitance C_P, and a series contact resistance R_S. The values of the circuit elements are found by inspection of Equation (6),

$$C = \frac{enN_0}{mV_t} W \times L, \qquad (7a)$$

$$R = \frac{1}{C} \frac{1}{\frac{1}{\tau_N} + v_{gr}\Gamma\ell S_0}, \qquad (7b)$$

$$L \simeq \frac{1}{C} \frac{\tau_S}{v_{gr}\Gamma\ell S_0} \frac{1}{1 - \tau_S v_{gr}\Gamma\varepsilon S_0 n}, \qquad (7c)$$

$$R_d \simeq L v_{gr}\Gamma\varepsilon S_0 n. \qquad (7d)$$

It also follows that the small-signal portion of the output power, P_1, is exactly proportional to the current I_L (Figure 4),

$$P_1 = \frac{hv}{e} \eta I_L, \qquad (8a)$$

with

$$\eta \simeq \frac{1}{2} \frac{\ln\left(\frac{1}{R}\right)}{\alpha L + \ln\left(\frac{1}{R}\right)}. \qquad (8b)$$

The differential quantum efficiency η is equal to the useful fraction of the photons, i.e., the fraction emerging through the front mirror.

Below threshold ($S_0 \simeq 0$), the RC time constant is the usual time constant of a diode; above threshold ($S_0 > 0$), the RC time constant is shortened because of stimulated recombination. This follows from Equation (7b), giving

$$\frac{1}{RC} = \frac{1}{\tau_N} + v_{gr}\Gamma\ell S_0. \qquad (9a)$$

It can be shown using Equations (1a), (3a), and (9a) that below threshold the following relationship between the RC time constant and the current density holds:

$$\left(\frac{1}{RC}\right)^2 = 4\bar{B}\left(\frac{J}{en}\right) + \frac{1}{\tau^2}. \qquad (9b)$$

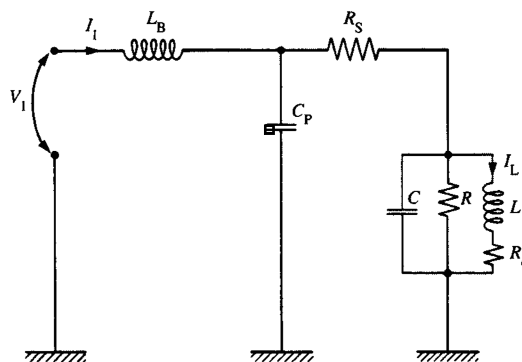

Figure 4

Equivalent circuit of a mounted single-quantum-well laser diode. L_B is the bond-wire inductance, C_P is the pad capacitance, R_S is the contact series resistance. The capacitor C, resistor R, inductor L, and resistor R_d represent the laser diode.

Measurements of this RC product at frequencies of a few hundred MHz and at current densities between 30 A-cm^{-2} and 300 A-cm^{-2} have confirmed this relationship and yielded the following values: $\bar{B} = 5 \times 10^{-5}$ cm^2-s^{-1} and $\tau = 2$–10 ns. Indications are that these values depend slightly on the number of QWs which are present.

The intrinsic modulation transfer function can easily be calculated using the equivalent circuit for a steady-state sinusoidal modulation as a function of the frequency ω ($L_B = C_P = R_S = 0$), viz:

$$\frac{P_1}{I_1} = \frac{hv}{e} \eta \frac{\frac{1}{LC}}{-\omega^2 + i\omega\gamma + \omega_r^2}, \qquad (10a)$$

where

$$\omega_r = \sqrt{\frac{1 + \frac{R_d}{R}}{LC}} \simeq \sqrt{\frac{v_{gr}\Gamma\ell S_0}{\tau_S}}, \qquad (10b)$$

and

$$\gamma = \frac{1}{RC} + \frac{R_d}{L} \simeq \frac{1}{\tau_N} + \omega_r^2\tau_S\left(1 + n\frac{\varepsilon}{\ell}\right). \qquad (10c)$$

This calculated modulation transfer function has a low-pass characteristic with a resonance at the relaxation frequency ω_r, a damping factor γ, and a second-order roll-off at high frequencies. A measured modulation transfer function is shown in **Figure 5**. Because the photodiode of the measurement system converts optical

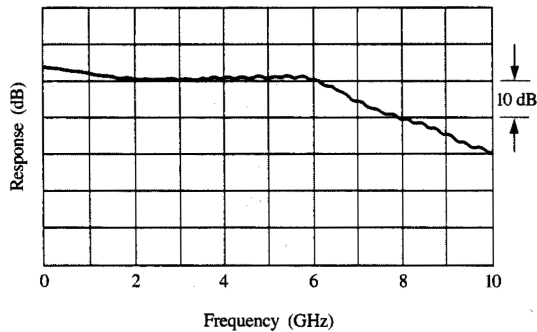

Figure 5

Measured small-signal response of the light output of a single-quantum-well laser diode. The diode is biased at 15 mW and has a length of 305 μm and a width of 4 μm.

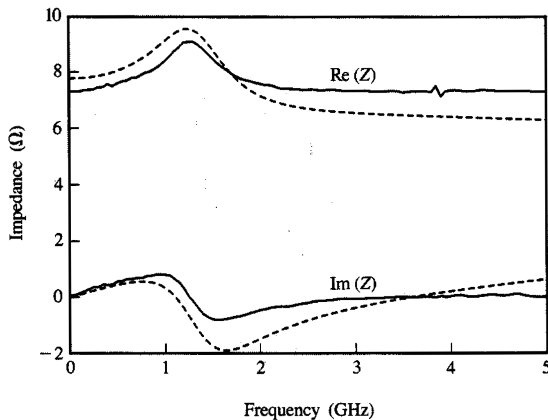

Figure 6

Measured (solid line) and calculated (dashed line) impedance Z of a single-quantum-well laser diode having a length of 600 μm and a width of 3 μm, biased at 1.5 mW. The calculations are based on the values listed in Table 1. The effects of L_B have been compensated for; $R_S = 6.7\ \Omega$, and $C_P = 1$ pF.

power into an electrical current, the second-order roll-off of Equation (10a) is seen having a 40-dB/decade slope.

The intrinsic impedance Z of the QW laser diode above threshold is very small due to the lasing process, but is not negligible, especially for diodes with very low threshold currents. By using the equivalent circuit we can calculate the impedance Z, where $L_B = C_P = R_S = 0$, to be equal to

$$Z(\omega) = \frac{V_1}{I_1} = \frac{\frac{R_d}{LC} + i\omega\frac{1}{C}}{-\omega^2 + i\omega\gamma + \omega_r^2}. \tag{11}$$

The impedance is small for both low and high frequencies and reaches its maximum around the relaxation frequency. The measured extrinsic impedance is shown in **Figure 6** as a function of the frequency, constituting the first measurement of the predicted effects of the relaxation resonance on the impedance of a single-QW laser diode. Also shown is the calculated impedance, based on Equation (11) and the values listed in Table 1.

- *High-speed modulation*

The bandwidth of a laser diode is very often limited by parasitic elements, especially those shown in Figure 4. To obtain high-speed performance, the resistance R_S was reduced to around 5 Ω with a very highly doped contact layer, the capacitance C_P was reduced to less than 1 pF by placing the bonding pad on a thick layer of polyimide with a low dielectric constant, as described in the section on fabrication, and the inductance L_B was reduced to below 0.5 nH by mounting the laser diode carefully in a high-speed package. With such low parasitics, the bandwidth of the single-QW laser diodes we examined was no longer limited by the parasitics at frequencies below 10 GHz, but by their intrinsic speed. The intrinsic upper limit of their useful bandwidth is thus given by the 0-dB bandwidth of the modulation transfer function—as can be derived from Equation (10a),

$$\omega_0 = \sqrt{2}\omega_r \sqrt{1 - \frac{1}{2}\left(\frac{\gamma}{\omega_r}\right)^2}$$

$$\simeq \sqrt{2} \sqrt{\frac{v_{gr}\ell\Gamma S_0}{\tau_S}\left[1 - \frac{1}{2}\frac{\ell S_0}{nG_0}\left(1 + n\frac{\varepsilon}{\ell}\right)\right]^2}. \tag{12}$$

This expression clearly states that the bandwidth of a laser can be increased by one or all of the following three means: increasing the differential gain constant, decreasing the photon lifetime, or operating the laser diode at high photon density in the quantum wells. In addition, the gain saturation parameter ε should be kept as small as possible. Note that the bandwidth does not depend strongly on the number of quantum wells, n (Γ is the confinement factor per quantum well and is the same for a single-QW laser diode as for a multi-QW laser diode).

The differential gain constant ℓ is a measure of how much the gain increases if the carrier density is increased, and depends critically on the density of states around the

quasi-Fermi levels of the electrons and holes. The differential gain constant in a quantum well can be much larger (up to a factor of four [10]) than in bulk material because of the steplike density of states in a quantum well. It can be further increased by proximity-doping the active region into a p-type region [11] and by changing the band structure using a strained active layer (12). Operating the laser diode at a lower temperature [13] also increases the bandwidth because of a sharpened carrier distribution and a concomitant increase of the differential gain constant.

A short photon lifetime τ_S can be obtained by reducing the mirror reflectivity R or by reducing the length L of the laser diode. A short photon lifetime increases the gain which is necessary to achieve lasing action [Equation (2a)]; since the maximum gain which can be obtained from one quantum well is limited, one must consider placing several quantum wells in the active region. A short photon lifetime also increases the threshold current. The power dissipated in the diode and resulting thermal effects would ultimately limit the practical lower limit of the photon lifetime [14]. This limit could of course be lowered through efficient heat-sinking or by restricting operation of the laser diode to a pulsed mode [15].

A high photon density ΓS_0 in one well can be obtained by operating the diode well above threshold. Ultimately limitations occur as a result of catastrophic optical mirror damage (COMD); this occurs in well-passivated QW laser diodes around power levels of 10 MW cm^{-2}, corresponding to $\Gamma S_0 \simeq 1 \times 10^{10}$ cm^{-2} for a quantum well with a thickness of 10 nm.

The relaxation resonance frequency as a function of the square root of the output power is shown in **Figure 7** for three single-QW laser diodes having different lengths. The predicted dependence of the relaxation frequency on power [Equation (12b)] is indeed observed. From the slopes we can derive an experimental differential gain constant of $\ell = 3\text{–}5 \times 10^{-10}$ cm.

At high power levels the bandwidth does not increase further with increasing output power because of gain saturation. At very high power levels, the bandwidth decreases with increasing output power, as can be inferred from Equation (12). The maximum 0-dB modulation bandwidth $\omega_{0,\max}$ is derived using Equation (12),

$$\omega_{0,\max} \simeq \frac{1}{\tau_S} \frac{1}{1 + n\dfrac{\varepsilon}{\ell}}. \qquad (13)$$

Using the values in Table 1 we find a maximum 0-dB modulation bandwidth for a device with one quantum well ($n = 1$) and a length $L = 300$ μm of $\omega_{0,\max} = 2\pi \cdot 8$ GHz. This value is very close to the actual measured maximum bandwidth of 6 GHz [see Figure 5].

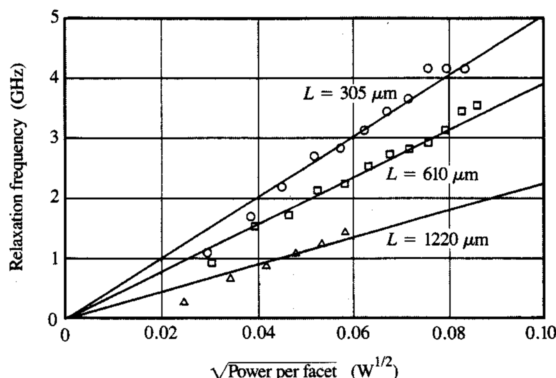

Figure 7

Relaxation frequency ω_r as a function of the square root of the optical power emitted through one facet, for three single-quantum-well laser diodes having different lengths.

In order to increase the maximum bandwidth, the strong modal gain saturation in these ridge quantum-well lasers must be overcome, e.g., through an improved lateral carrier confinement.

- *Large-signal modulation*

In digital communication systems, data transmission by means of a laser diode usually requires turning the diode completely on and off. The large-signal modulation behavior of a laser diode is therefore of much more practical interest than the small-signal response. However, due to the highly nonlinear characteristic of a laser diode (as can easily be seen from the rate equations), it is very difficult to develop a general description of the pulse response of such a diode. The response depends strongly on the bias and the signal amplitude, and only highly simplified models exist [16]. In **Figure 8** we show the response of a single-QW laser diode with a threshold current of 8 mA. The diode had been subjected to square-wave current switching between 8 mA and 20 mA, with a period of 1 ns and a rise time and fall time of approximately 60 ps. The rise time and fall time of the light output were found to be 65 ps and 215 ps, respectively. The diode switches on more rapidly than off because it is biased around the threshold current. Not prebiasing the diode increases the switching-on time considerably, whereas the switching-off time remains essentially unaffected. This undesirable dependence on the biasing condition can be reduced substantially by reducing the threshold current. Recently, single-QW laser diodes with threshold currents only marginally larger than 0.5 mA have been demonstrated [16]; such diodes

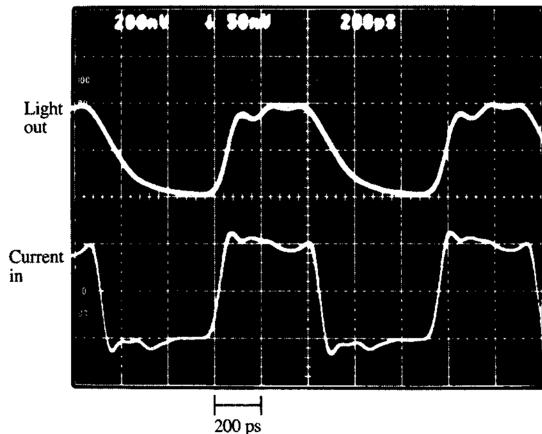

Figure 8

Large-signal response of a single-quantum-well laser diode with a threshold current of 8 mA. The drive current is switched between 8 mA and 20 mA; associated rise and fall times are 65 ps and 215 ps, respectively.

are very attractive for digital communication applications. The quest for lower threshold currents has given rise to efforts in laser diode scaling, through which it should be possible to reduce further the threshold current [17].

High-speed photodetectors

• *GaAs metal–semiconductor–metal photodiodes*
Although traditionally PIN (p-doped/intrinsic/n-doped) photodiodes and APD (avalanche photodiodes) have been the preferred optoelectronic detectors for use in fiber communication systems, the GaAs metal–semiconductor–metal (MSM) photodiode has emerged as a viable alternative. Initially there was little difference in performance between a photoconductor and an MSM photodiode. But its ease of fabrication proved to be motivation to gradually improve its efficiency, dark current, and bandwidth, making it comparable to a PIN diode. The full potential of the MSM photodiode became evident through the monolithic integration with GaAs MESFETs, resulting in high-speed optoelectronic receivers. Recent results show that the electronic components rather than the detector are limiting factors in such receivers; hence further advances can be expected.

When comparing the GaAs MSM diode with other photodiodes, we use as figures of merit the photodiode efficiency and the diode capacitance. It can be shown that for a single-stage integrating receiver, the responsivity–bandwidth product is proportional to $\eta/(C_{PD} + C_{IN})$, where η is the overall efficiency of the diode, C_{PD} is the photodiode capacitance, and C_{IN} is the input capacitance of the amplifier. On the other hand, the highest sensitivity of the receiver is obtained for the smallest diode capacitance and lowest leakage current (dark current) [18, 19].

The capacitance of an MSM diode is only one quarter that of a PIN diode having the same photosensitive area [20]. Hence, despite the <50% lower efficiency due to blocking of the incoming light with its metal fingers, the MSM diode combined with an integrating receiver would be expected to double the responsivity–bandwidth product which could be obtained using a PIN diode.

An additional advantage of the MSM diode is its simple structure: The diode can be integrated on a chip with high-speed GaAs circuits with relatively minor fabrication modifications, in most cases without adding additional lithography steps. This monolithic integration eliminates the parasitic bond inductance and pad capacitance of a hybrid combination of photodiode and amplifier, which, together with the low-noise and high-speed MESFETs or HEMTs, provides an ideal means for fabricating high-performance optical receivers [21–23]. The monolithic integration should eventually lead to the possibility of low-cost receiver arrays.

The structure of a GaAs MSM photodiode is shown in **Figure 9**. It consists of a set of interdigitated metal fingers on a GaAs substrate, resulting in a large-active-area diode with a short spacing between the electrodes. Its principle of operation is as follows: Photons incident on the GaAs surface create electrons and holes which travel along the field lines to the contacts. In order to limit the dc current when no light is present, the contacts are formed as Schottky barrier contacts. The energy-band structure illustrates the flow of photon-generated electrons and holes within the device and shows how the Schottky barriers prevent injection of carriers from the contacts into the semiconductor.

Early devices were reported to have gain, some even at high frequencies. We distinguish between two possible gain mechanisms:

- Gain due to avalanche multiplication. As in the case of a regular avalanche photodiode, gain can be obtained because of avalanche multiplication of carriers in the high-field region of the device. Sharp edges at the contacts of the MSM detector would favor creation of high fields. As for an APD, a high voltage must be applied and a uniform drift region must be obtained to avoid breakdown.
- Gain due to trapping of holes (or electrons) close to the Schottky contact. Hole (or electron) accumulation

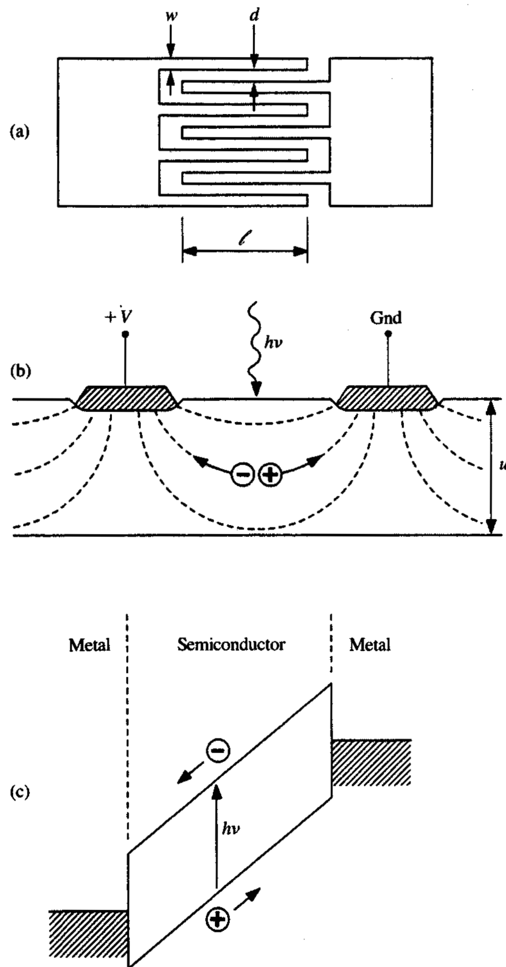

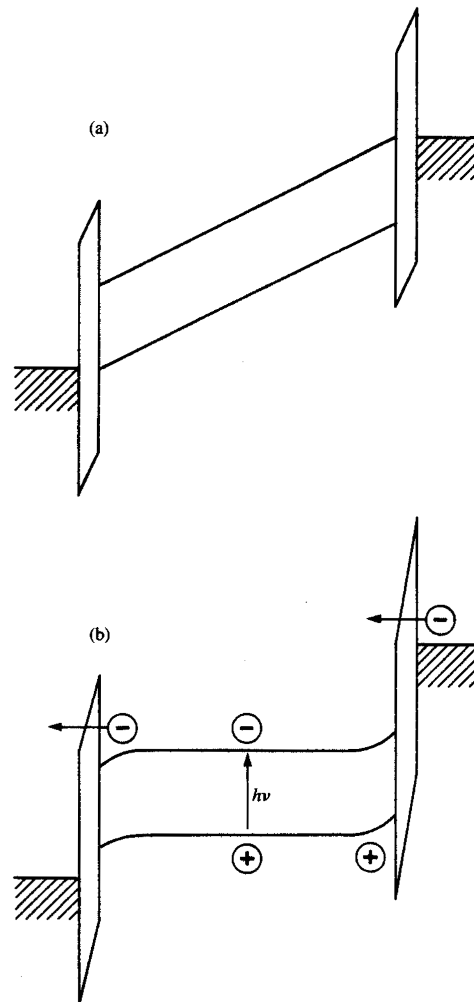

Figure 9

(a) Geometry of a GaAs MSM photodiode with finger length ℓ, width w, and distance between fingers d. (b) Cross section illustrating the generation by photons of electrons and holes which flow along field lines (dotted) toward the contacts. The height of the photosensitive region u is also indicated. (c) Associated energy-band structure.

Figure 10

Illustration of the gain mechanism due to thin barriers at the Schottky contacts. Energy-band structure (a) without illumination and (b) with illumination. Holes accumulate at the barrier and cause injection of electrons from the metallic contact into the semiconductor.

increases the field at the contact, which in turn increases injection of electrons (or holes) into the semiconductor, resulting in current gain. This effect occurs at relatively low frequencies depending on the nature of the trapping mechanism. A tunnel barrier at the contact (for instance, a thin oxide layer) has a similar effect, as shown schematically in **Figure 10**: Holes are accumulated at the interface between the barrier and the semiconductor and cause additional electron injection into the semiconductor by increasing the field across the barrier. It should be noted that depending on the nature of the barrier, the electron injection occurs through field-dependent tunneling, thermionic emission, or a combination of both.

Provided it is controlled and not strongly frequency-dependent, gain is certainly a desirable feature. Avalanche gain can be used provided the lateral avalanche mechanism can be controlled reliably. The nonuniform field within the MSM diode makes it difficult to obtain high gain and still avoid breakdown. It should be noted that to first order, the gain–bandwidth

product of an avalanche photodiode is gain-independent, so that in combination with an integrating amplifier, its performance is similar to that of an MSM photodiode.

On the other hand, gain mechanisms with low cutoff frequency are undesirable when used in a high-speed receiver. These can be prevented by reducing trap densities, especially at the exposed GaAs surface, by avoiding high fields at the contacts which favor electron injection (this also reduces the leakage current), and by fabricating high-quality Schottky diodes without an interfacial layer. Rogers [22, 24] eliminated the low-frequency gain by adding a fixed background charge (an enhancement transistor channel which is fully depleted by the surface potential), making the field distribution less sensitive to trapped charge.

Efficiency of the MSM photodiode is an important issue, because any loss in the detector needs to be compensated by an increased gain of the amplifier. A typical amplifier has a constant gain–bandwidth product, so a higher gain implies a lower bandwidth. More gain can also be obtained without bandwidth reduction by cascading several amplifiers at the expense of increased complexity and power dissipation. The efficiency of an MSM diode is given by

$$\eta = (1 - r)\frac{d}{d + w}(1 - e^{-u/\lambda}), \tag{14}$$

where r is the transmission at the GaAs–air interface, d the finger spacing, w the finger width, u the thickness of the absorbing section, and λ the absorption length. This differs mainly from a PIN diode because part of the active area is blocked by the metal fingers.

The use of transparent Schottky contacts (indium tin oxide) has been proposed [25] to increase the efficiency. The disadvantage of this approach is that carriers are generated in the low-field region under the contact, affecting high-speed behavior. The same is true for structures with $d \ll u$, where the short finger spacing increases the transit time of the carriers created deep in the GaAs. As in the case of a PIN diode, the efficiency can also be increased (by 30%) by depositing an antireflection coating on the MSM photodiode. Such a coating might also serve as a passivation layer to protect the surface against oxidation.

Next we describe the fabrication of a very high-speed MSM photodiode, its dc characteristics and high-speed measurement, and present a comparison with calculations. We then discuss further directions and applications.

Fabrication

In an attempt to obtain the limiting bandwidth for an MSM diode, three aspects of the diode were given special attention: 1) Its capacitance was kept low by making its surface area small (10 μm by 15 μm). 2) A short carrier transit time was obtained by reducing the distance between the fingers to 0.5 μm. 3) It was connected to an on-chip tapered coplanar line which provided an impedance-matched transition to the coplanar transmission line of the picosecond measurement system.

The diodes were fabricated on an undoped 1-μm-thick GaAs MBE-grown buffer layer. The buffer layer was separated from the GaAs substrate by a GaAs/AlAs superlattice. Above the buffer layer was a 30-nm-thick, 9×10^{16}-cm^{-3} beryllium-doped layer which was fully depleted by the surface potential. The purpose of that layer was to make the field at the surface less susceptible to trapped charge—by fixing the field by means of a high background doping density level. The Schottky contact was fabricated as follows: using a double-layer PMMA (each layer having a different molecular weight), we obtained a very good lift-off pattern after electron-beam exposure and development [26]. Resist residues were removed in an oxygen plasma. Then 50 nm of GaAs was removed using a 1:8:1000 H_2SO_4:H_2O_2:H_2O etch solution. This is an isotropic etch which creates rounded corners at the edge of the contact, thereby preventing the formation of high fields. Before depositing the 120-nm-thick aluminum Schottky contact, the oxide at the GaAs surface was removed using 1:1 HCl:H_2O. This cleaning step was shown to improve the Schottky diode ideality factor substantially on highly doped epitaxial layers [27]. Fabrication was completed by depositing a 300-nm-thick aluminum layer from which the tapered coplanar line was formed.

dc characteristics

The dc characteristics of a typical MSM diode having 1-μm spacing between its fingers are shown in **Figure 11**. The current through the diode is displayed as a function of applied voltage for different light intensities. As expected from the symmetry of the structure, the characteristics are point-symmetric around zero. The diode can therefore be used with either a positive or a negative bias, and yields the same signal but with opposite polarity [28]. We also distinguish between two regions: the region around zero, where the current is strongly voltage-dependent (the linear region, $V < 1$ V) and the region at higher voltages where the current saturates with voltage (the saturated region, $V > 1$ V).

The measured current is a result of three different and competing effects: carrier diffusion, carrier drift, and carrier recombination. In the linear regime each of the three components plays a role in causing a rapid rise of current with voltage; in the saturated regime almost all carriers are swept out to the contacts before they can be lost either by diffusion or recombination. The remaining nonzero slope in the I–V curve is due to carriers which

are generated in a low field region of the detector; therefore they require a longer transit time to reach the contact and are more likely to be lost by recombination. An increase in voltage reduces the number of carriers lost by recombination and increases the total current.

The diodes typically have a leakage current of 1 nA at 4 V just after fabrication. This low leakage current is attributed to their small size and to the quality of the Schottky barrier. Without a passivation layer this leakage current increases with time to 0.1–1 μA; we attribute this to surface conduction caused by the oxidation of the GaAs surface. Maximum sensitivity ranges between 0.1 and 0.2 A/W at 830 nm for diodes without antireflection coating.

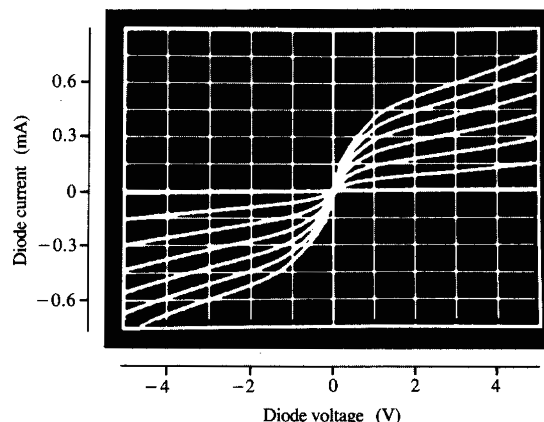

Figure 11

Current–voltage characteristics of a typical GaAs MSM photodiode for light intensities ranging from 0 to 6 mW at 830 nm. Finger spacing was 1 μm.

• *High-speed behavior*

The capacitances of the MSM diodes were determined from *S*-parameter measurements at 4 GHz. A capacitance of 12 fF or 0.1 fF/μm finger length was obtained, which is in agreement with the theoretical value discussed by Ito and Wada [20]. In a preliminary high-speed measurement, an MSM photodiode was mounted on a Wiltron *K*-connector and illuminated with 16-ps 830-nm pulses from a current-spiked commercial laser diode. The electrical signal was monitored with a Hewlett-Packard 54120T sampling oscilloscope. A full width half maximum (FWHM) of 24 ps, mainly determined by the sampling oscilloscope, was obtained.

The high-speed measurement arrangement used is shown in **Figure 12**. It consists of a GaAs chip containing the photodiode and the tapered coplanar line, which is wire-bonded to a silicon-on-sapphire (SOS) chip containing a long coplanar line having a 50-μm line width and 50-μm spacing. The signal on the coplanar line was measured using SOS photoconductive switches whose response time was reduced by ion bombardment of the silicon [29]. The sampling experiment was then performed by applying a 1.8-ps laser pulse from a frequency-doubled YAG laser with fiber pulse compression to the photodiode and a second pulse with variable delay to the photoconductive switch. The output signal was the average current through the photoconductor as a function of the delay between the two pulses. The repetition rate of the pulses was 100 MHz, the average power applied to the diode 46 μW, and the wavelength 532 nm.

The sampling measurement yielded an FWHM of 4.8 ps for a bias voltage of 0.5 V, as shown in **Figure 13(a)**. The experimental result is also compared to a one-dimensional numerical calculation [30] which is discussed in more detail below. By deconvolution of the diode impulse response with that of the measurement system and subsequent Fourier transformation, the intrinsic frequency response of the photodiode was obtained. The resulting −3-dB bandwidth was 105 GHz, which is the highest bandwidth thus far reported for an MSM photodiode [31].

The 5-ps FWHM described above was measured at a wavelength of 532 nm. At 830 nm one would expect a distinctly slower response due to the large penetration depth of the light into the semiconductor (≃1 μm). However, by adding a buried AlGaAs layer the generation of carriers in the low-field region can be eliminated, but at the cost of efficiency [32]. A similar wavelength-dependent trade-off between transit time and efficiency exists for high-speed PIN diodes [33].

In our search for transit-time effects we studied the pulse response while varying the bias voltage. Compared to the pulse at a 0.5-V bias, the pulse amplitude at a 0.05-V bias was only 20% lower, and the FWHM increased from 4.8 to 6 ps. This confirms that parasitic elements rather than transit-time effects dominate the response, and that the diodes have a very large bandwidth at low bias voltage. The symmetric structure of the diode allows the electrical signal on the line to be reversed simply by reversing the polarity of the supply voltage, an effect which we observed experimentally for 5-ps pulses.

Modeling

The calculated curve in Figure 13(a) was based on a one-dimensional model of the MSM diode which takes into account carrier drift and diffusion, field-dependent mobility for the electrons, and recombination of carriers though recombination centers. The use of a one-

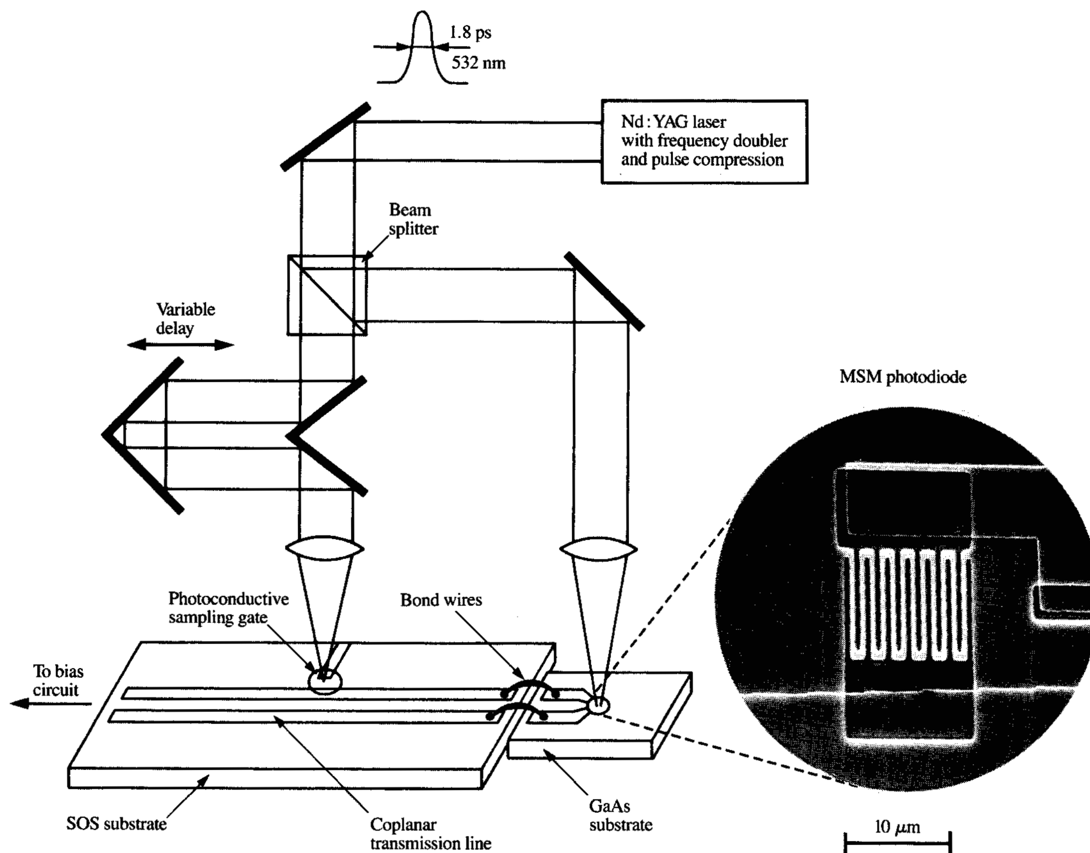

Figure 12

High-speed measurement arrangement. The MSM photodiode is coupled to a coplanar transmission line, and the signal is measured using a photoconductive sampling gate.

dimensional model is justified because of the short absorption length (100 nm) compared to the finger spacing (500 nm). For a detailed analysis of a two-dimensional calculation, we refer the reader to Reference [34]. The continuity equations for electrons and holes were solved consistently with Poisson's equation. Parasitic elements were included in the calculation by means of circuit equations; the equivalent circuit is shown in **Figure 13(b)**. A Gaussian input pulse with $1.8 \times \sqrt{2}$ ps FWHM was used to simulate the width of the optical pulses in the actual measurement.

A first and crucial observation was that solely the electrons generated in the GaAs are responsible for the picosecond response of the MSM photodiode. Due to the difference between electron and hole mobility and the short recombination time at the surface, the pulse response without parasitic elements present consists of a first initial peak caused by the electrons followed by a long tail caused by the holes. Since the holes remain longer in the structure than do the electrons, they are more likely to recombine or become trapped. The frequency response therefore has two transitions: one due to the long transit time of the holes, which causes a 6-dB drop around the hole transit frequency, and the second, caused by the electrons. Because of the very low surface mobility of the holes in our experiment (measured to be 100 cm^2/V-s), this 6-dB drop was at frequencies below 10 GHz and thus outside the range of our high-speed measurement. The 6-dB loss in sensitivity must be taken into account to obtain the high bandwidth.

The calculation also confirmed that parasitic elements rather than transit-time effects dominated the measured

impulse response. When subtracting the finite pulse width of the applied pulses and the bond inductance of the measurement arrangement to obtain the bandwidth of the intrinsic detector (as discussed above), the high-frequency roll-off was found to be caused almost equally by 1) the 1.2-ps RC time constant of the diode capacitance and transmission line impedance and 2) the 1.6-ps average electron transit time.

Using the model we also explored different design trade-offs. For example, by reducing the RC time constant by further reducing the size of the diode and hence its capacitance (5 fF), using a lower transmission line impedance (50 Ω), and reducing the transit time with a shorter finger spacing (0.25 μm), we calculated a pulse response with a FWHM below 1 ps.

For such short response times one must question the validity of the model. Nonstationary carrier dynamics should be included in the calculation. For transit times of 1 ps and less, an enhanced carrier velocity [35] (the so-called velocity overshoot) would be expected which would lead to an even shorter pulse response of the MSM photodiode. It would therefore also be a useful tool for studying velocity overshoot effects. A first calculation of this sort was published by Koscielniak et al. [36], although detailed theoretical analysis and comparison with experiment still remain to be done. The same authors also took a first step toward analyzing quantum-mechanical effects; as dimensions are reduced and the transit times become smaller than any scattering time within the device, macroscopic quantum-mechanical effects should become more pronounced.

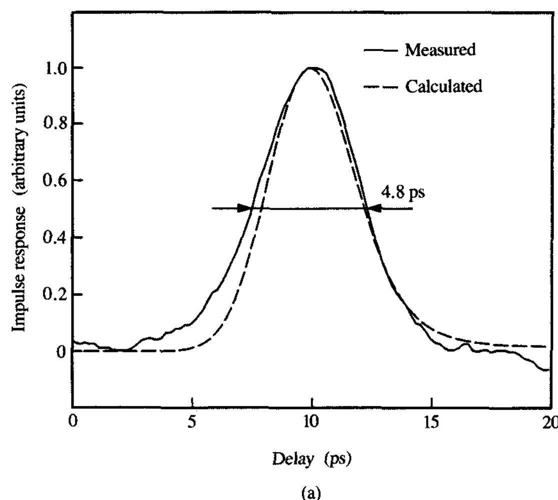

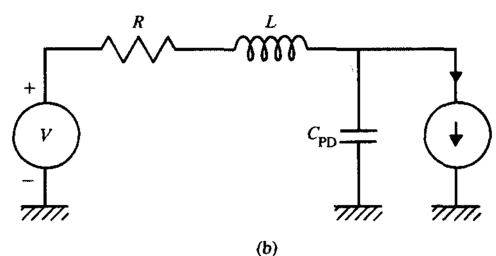

Figure 13

(a) Impulse response of a GaAs MSM photodiode with a 0.5-μm finger spacing (solid line) compared to the calculations (dotted line). (b) Equivalent circuit used for impulse response calculation. Assumed values: L = 100 fH, C_{PD} = 12 fF, and R = 100 Ω.

Future directions and applications

One possibility considered has been the application of the same device concept to a different material such as GaInAs, which is sensitive to 1.3-μm-wavelength light, which is of prime importance for long-distance telecommunication. However, to succeed in that regard will require the development of means to obtain good-quality Schottky barriers using that material—possibly by using a strained GaAs contact layer or an AlGaAs/AlInAs superlattice with a variable ratio of the two constituents [37, 38]. This material is also of interest at a wavelength of 0.8 μm, since it has a shorter absorption length than GaAs and its carriers have a greater room-temperature mobility. Both advantages should improve the efficiency-bandwidth product of the detector.

The simple structure and the high performance of the MSM photodiode make it very attractive for integrated optoelectronic receivers. Its low capacitance allows integrating receivers to be fabricated with a high input impedance and large gain in a single stage without limiting bandwidth. An alternate approach for micro- and millimeter wave applications may be to combine the MSM photodiode with a traveling wave amplifier. This arrangement might lead to a receiver bandwidth as large as the detector bandwidth, provided transistors with a sufficiently high transit frequency could be used.

Another application is that of mixing and sampling. The steep voltage dependence shown in Figure 11 allows an electrical signal to be sampled by applying a short light pulse to the detector. The time resolution is limited by the response time of the detector. Compared to ion-bombarded photoconductive switches, the MSM photodiode has a larger sensitivity–bandwidth product, since the short response time is not obtained at the expense of carrier mobility [29]. Mixing an electrical and an optical signal is the equivalent of sampling in the frequency domain. An interesting application would be the demultiplexing within the photodiode of a frequency-

multiplexed signal, with the potential advantage being that it would require a lower-bandwidth preamplifier.

Summary

We have presented an overview, mainly of work in our laboratory, of high-speed GaAs/AlGaAs ridge-waveguide quantum-well laser diodes, including their fabrication, associated rate equations, and small-signal equivalent circuit. In addition, we have presented experimental results on their high-speed small-signal as well as large-signal modulation. The low threshold, high efficiency, low temperature sensitivity, and high-speed modulation capability at low power levels of the ridge-waveguide single-quantum-well laser diode make it a very attractive light-emitting device for short-distance data communication.

We have also presented an overview of the GaAs metal–semiconductor–metal photodiode, including its fabrication, principles of operation, different gain mechanisms, and overall efficiency. In addition, we have presented some new results on its dc and high-speed characteristics, and on a relevant comparison with a drift diffusion model. Its relatively simple structure, low bias voltage operation, and excellent high-speed performance make this type of photodiode potentially attractive for high-speed monolithic optoelectronic receivers as well as monolithic micro- and millimeter-wave optoelectronic circuits.

Together with GaAs MESFET circuits, the above devices are at present the primary choice for light emission and detection in integrated, high-performance and very compact multi-channel links for optical data transmission within and between digital computer systems.

Acknowledgments

We would like to thank Bob Melcher for his continued encouragement, the LST department of our laboratory for their excellent technical support, W. Patrick for the fabrication of the photodetectors, and J. M. Halbout for the impulse response measurements.

References and notes

1. John D. Crow, C. J. Anderson, S. Bermon, A. Callegari, John F. Ewen, J. D. Feder, J. H. Greiner, E. P. Harris, Peter D. Hoh, H. J. Hovel, J. H. Magerlein, T. E. McKoy, A. T. S. Pomerene, Dennis L. Rogers, G. J. Scott, M. Thomas, G. W. Mulvey, B. K. Ko, Tokeo Ohashi, M. Scontras and D. Widiger, "A GaAs MESFET IC for Optical Multiprocessor Networks," *IEEE Trans. Electron Devices* **36,** 263 (February 1989).
2. See for example R. D. Dupuis, "An Introduction to the Development of the Semiconductor Laser," *IEEE J. Quantum Electron.* **QE-23,** 651 (1987) for a brief review of experimental and theoretical work on the semiconductor diode laser.
3. K. C. Kao and G. A. Hockham, "Dielectric Fiber Surface Waveguides for Optical Frequencies," *Proc. IEEE* **113,** 1151 (1966).
4. A. Yariv, "The Beginning of Circuits," *IEEE Trans. Electron Devices* **ED-31,** 1656 (1984).
5. W. Tsang, "Extremely Low Threshold (AlGa)As Graded-Index Waveguide Separate-Confinement Heterostructure Lasers Grown by Molecular Beam Epitaxy," *Appl. Phys. Lett.* **40,** 217 (1982).
6. C. Harder, P. Buchmann, and H. Meier, "High-Power Ridge-Waveguide AlGaAs GRIN-SCH Laser Diode," *Electron. Lett.* **22,** 1081 (1986).
7. F. Sato, H. Imamato, M. Asai, T. Inoue, K. Imanaka, and M. Shimura, "Low Thermal Expansion Polyimide Buried Ridge Waveguide AlGaAs Single-Quantum-Well Laser Diode," *J. Appl. Phys.* **63,** 964 (1988).
8. Ch. Harder, J. Katz, S. Margalit, J. Shacham, and A. Yariv, "Noise Equivalent Circuit of a Semiconductor Laser Diode," *IEEE J. Quantum Electron.* **QE-18,** 333 (1982).
9. H. C. Casey, Jr. and M. B. Panish, *Heterostructure Lasers, Part A: Fundamental Principles,* Academic Press, London, 1978, p. 52.
10. Y. Arakawa and A. Yariv, "Theory of Gain, Modulation Response, and Spectral Linewidth in AlGaAs Quantum-Well Lasers," *IEEE J. Quantum Electron.* **QE-21,** 1666 (1985).
11. K. J. Vahala and C. E. Zah, "Effect of Doping on the Optical Gain and the Spontaneous Noise Enhancement Factor in Quantum-Well Amplifiers and Lasers Studied by Simple Analytical Expressions," *Appl. Phys. Lett.* **52,** 1945 (1988).
12. I. Suemune, L. A. Coldren, M. Yamanishi, and Y. Kan, "Extremely Wide Modulation Bandwidth in a Low Threshold Current Strained Quantum-Well Laser," *Appl. Phys. Lett.* **53,** 1378 (1988).
13. K. Y. Lau, Ch. Harder, and A. Yariv, "Direct Modulation of Semiconductor Lasers at $f > 10$ GHz by Low-Temperature Operation," *Appl. Phys. Lett.* **44,** 273 (1984).
14. J. E. Bowers, "High Speed Semiconductor Laser Design and Performance," *Solid-State Electron.* **30,** 1 (1987).
15. K. Uomi, N. Chinone, T. Ohtoshi, and T. Kajimura, "High Relaxation Oscillation Frequency (Beyond 10 GHz) of GaAlAs Multiquantum-Well Lasers," *Jpn. J. Appl. Phys.* **24,** L539 (1985).
16. K. Y. Lau, N. Bar-Chaim, P. L. Derry, and A. Yariv, "High Speed Digital Modulation of Ultralow Threshold (<1 mA) GaAs Single Quantum-Well Lasers Without Bias," *Appl. Phys. Lett.* **51,** 69 (1987).
17. E. Marclay, D. J. Arent, C. Harder, H. P. Meier, W. Walter, and D. J. Webb, "Scaling of GaAs/AlGaAs Laser Diodes for Submilliampere Threshold Current," *Electron. Lett.* **25,** 892 (1989).
18. D. P. Schinke, R. G. Smith, and A. R. Hartman, "Photodetectors," *Semiconductor Devices for Optical Communication,* Springer-Verlag, New York, 1980, Ch. 3.
19. R. G. Smith and S. D. Personick, "Receiver Design for Optical Fiber Communication Systems," *Semiconductor Devices for Optical Communication,* Springer-Verlag, New York, 1980, Ch. 4.
20. M. Ito and O. Wada, "Low Dark Current GaAs Metal–Semiconductor–Metal (MSM) Photodiodes Using WSi_x Contacts," *IEEE J. Quantum Electron.* **QE-22,** 1073 (1986).
21. M. Ito, T. Kumai, H. Hamaguchi, M. Makiuchi, K. Nakai, O. Wada, and T. Sakurai, "High-Speed Monolithically Integrated GaAs Photoreceiver Using a Metal–Semiconductor–Metal Photodiode," *Appl. Phys. Lett.* **47,** 1129 (1985).
22. D. L. Rogers, "Monolithic Integration of a 3-GHz Detector/Preamplifier Using a Refractory-Gate, Ion-Implanted MESFET Process," *IEEE Trans. Electron Device Lett.* **EDL-7,** 600 (1986).
23. Ch. S. Harder, B. J. Van Zeghbroeck, H. Meier, W. Patrick, and P. Vettiger, "5.2 GHz Bandwidth Monolithic GaAs Optoelectronic Receiver," *IEEE Trans. Electron Device Lett.* **9,** 171 (1988).
24. D. L. Rogers, "MESFET Compatible IMSM Detectors," *Proceedings of the Picosecond Electronics and Optoelectronics Conference,* Salt Lake City, UT, January 1987, p. 116.

25. M. Zirngibl, R. Sachot, W. Baer, and M. Ilegems, "High Sensitive and Fast Photodetectors at 820 nm," *Helv. Phys. Acta* **61,** 845 (1988).
26. S. Mackie and S. P. Beaumont, "Materials and Processes for Nanometer Lithography," *Solid State Technol.* **28,** 117 (1985).
27. W. Patrick, K. Dätwyler, B. J. Van Zeghbroeck, and P. Vettiger, "Technology for Submicron Recessed Gate GaAs MESFETs on Thin MBE Layers Using Electron-Beam Lithography," *Proceedings of the International Symposium on GaAs and Related Compounds,* Heraklion, Greece, 1987, IOP Publishing Ltd., Institute of Physics Conference Series No. 91, Ch. 7, p. 637.
28. W. Roth, H. Schumacher, J. Kluge, H. J. Geelen, and H. Beneking, "The DSI Diode—A Fast Large-Area Optoelectronic Detector," *IEEE Trans. Electron Devices* **ED-32,** 1034 (1985).
29. P. R. Smith, D. H. Auston, A. M. Johnson, and W. M. Augustyniak, "Picosecond Photoconductivity in Radiation-Damaged Silicon-on-Sapphire Films," *Appl. Phys. Lett.* **38,** 47 (1981).
30. B. J. Van Zeghbroeck, "Analysis of Picosecond and Subpicosecond MSM Photodiodes with Very Low Bias Voltage," presented at the Device Research Conference, Boulder, Colorado, 1988.
31. Other types of Schottky barrier photodiodes with a similar bandwidth have been reported, e.g., S. Y. Wang and D. M. Bloom, "100 GHz Bandwidth Planar GaAs Schottky Photodiode," *Electron. Lett.* **19,** 554 (1983); and D. G. Parker, P. G. Say, and A. M. Hansom, "110 GHz High-Efficiency Photodiodes Fabricated from Indium Tin Oxide/GaAs," *Electron. Lett.* **23,** 527 (1987).
32. L. Figueroa and C. W. Slayman, "A Novel Heterostructure Interdigital Photodetector with Picosecond Optical Response," *IEEE Trans. Electron Device Lett.* **EDL-2,** 208 (1981).
33. J. E. Bowers and C. A. Burris, "Ultrawide-Band Long-Wavelength p-i-n Photodetectors," *J. Lightwave Technol.* **LT-5,** 1339 (1987).
34. R. L. Peterson, "Numerical Study of Currents and Fields in a Photoconductive Detector," *IEEE J. Quantum Electron.* **QE-23,** 1185 (1987).
35. J. G. Ruch, "Electron Dynamics in Short Channel Field-Effect Transistors," *IEEE Trans. Electron Devices* **ED-19,** 652 (1972).
36. W. C. Koscielniak, J. L. Pelouard, and M. A. Littlejohn, "Dynamic Behavior of Photocarriers in a GaAs Metal–Semiconductor–Metal Photodetector with Sub-Half-Micron Electrode Pattern," *Appl. Phys. Lett.* **54,** 567 (1989).
37. D. L. Rogers, J. M. Woodall, G. D. Pettit, and D. McInturff, "High-Speed 1.3 μm GaInAs Detectors on GaAs Substrates," *IEEE Trans. Electron. Device Lett.* **9,** 515 (1988).
38. O. Wada, H. Nobuhara, H. Hamaguchi, T. Mikawa, A. Tackeuchi, and T. Fuji, "Very High-Speed GaInAs Metal–Semiconductor–Metal Photodiode Incorporating an AlInAs/GaInAs Graded Superlattice," *Appl. Phys. Lett.* **54,** 16 (1989).

Received June 2, 1989; accepted for publication November 6, 1989

Christoph S. Harder *IBM Research Division, Zurich Research Laboratory, Säumerstrasse 4, 8803 Rüschlikon, Switzerland.*

Dr. Harder received his Electrical Engineering Diploma from the Eidgenoessische Technische Hochschule in Zurich in 1978. He received his M.S. and Ph.D. degrees, both in electrical engineering, from the California Institute of Technology in 1980 and 1983, respectively. He then joined the IBM Research Laboratory in Zurich, initially to work on the GaAs MESFET technology. In 1986, Dr. Harder started the work in that laboratory on optoelectronic technology. Since 1988 he has been the manager of the Optical Interconnection Device Group in the Laser Science and Technology Department. His current interests include ultra-low-threshold and high-speed lasers, as well as semiconductor laser device physics. Dr. Harder is a member of the Institute of Electrical and Electronics Engineers and the American Physical Society.

Bart J. Van Zeghbroeck *Department of Electrical and Computer Engineering, and the Optoelectronic Computing Systems Center, University of Colorado, Boulder, Colorado 80309.*

Dr. Van Zeghbroeck received an Electrical Engineering Diploma from the Catholic University of Leuven, Belgium, in 1980. He received his M.S. and Ph.D degrees, both in electrical engineering, from the University of Colorado at Boulder in 1981 and 1984, respectively. From 1981 through 1984, he was affiliated with the National Institute of Standards and Technology (formerly the National Bureau of Standards) in Boulder, where he worked on superconducting devices with gain, and sampling and logic circuits. From 1984 to 1990 Dr. Van Zeghbroeck was at the IBM Zurich Research Laboratory, where he worked on submicron recessed-gate GaAs MESFETs, high-speed photodiodes and receivers, and semiconductor lasers. Since the beginning of 1990 he has been with the University of Colorado at Boulder, as an Associate Professor in the Department of Electrical and Computer Engineering, and the Optoelectronic Computing Systems Center. Dr. Van Zeghbroeck is a member of the Institute of Electrical and Electronics Engineers.

Morris P. Kesler *IBM Research Division, Zurich Research Laboratory, Säumerstrasse 4, 8803 Rüschlikon, Switzerland.*

Dr. Kesler received his B.S. and M.S. degrees in electrical engineering in 1984, and his Ph.D. degree in electrical engineering in 1988, each from the Massachusetts Institute of Technology. His doctoral research pertained to the measurement of ultrafast dynamics in semiconductor lasers using femtosecond optical pulses. He is currently a Postdoctoral Fellow at the IBM Zurich Research Laboratory, where he is investigating fundamental properties of quantum-well lasers. Dr. Kesler is a member of Sigma Xi, the Optical Society of America, and the IEEE Lasers and Electro-Optics Society.

Heinz P. Meier *IBM Research Division, Zurich Research Laboratory, Säumerstrasse 4, 8803 Rüschlikon, Switzerland.*

Dr. Meier received a Diploma in inorganic chemistry and a Ph.D. in physical chemistry from the University of Zurich in 1981 and 1984, respectively. He then joined the IBM Research Laboratory in Zurich, initially to work on the GaAs MESFET technology. Since 1985, Dr. Meier has worked on crystal growth by MBE. His interests have included optoelectronic devices such as low-threshold GaAs/AlGaAs lasers, strained-layer lasers, and growth over nonplanar substrates. Since 1989 he has been the manager of the MBE Group in the Laser Science and Technology Department. His current interests include the CBE growth of phosphorus compound semiconductor lasers. Dr. Meier is a member of the American Physical Society.

Peter Vettiger *IBM Research Division, Zurich Research Laboratory, Säumerstrasse 4, 8803 Rüschlikon, Switzerland.*

Mr. Vettiger received his Diploma in Electrical Engineering from the

Zurich State Engineering School in 1966. He joined the IBM Zurich Research Laboratory in 1963 to work on concept and circuit designs for high-speed A/D converters, digital encoding of voice and image sources, and data transmission. In 1978 he was on a one-year assignment in the Electron-Beam Lithography Department of the IBM Thomas J. Watson Research Center, Yorktown Heights, New York. Since 1979 he has been involved in nanometer fabrication activities for Josephson tunneling devices, and submicron GaAs MESFETs and opto-electronic devices. In 1983 Mr. Vettiger became responsible for the Device Lithography Group and is currently manager of the Materials and Process Technology Groups in the Laser Science and Technology Department. His current interests are in the processing technology and nanometer patterning aspects of fabricating semiconductor lasers and related devices for optoelectronic integration. Mr. Vettiger is a member of the Institute of Electrical and Electronics Engineers.

David J. Webb *IBM Research Division, Zurich Research Laboratory, Säumerstrasse 4, 8803 Rüschlikon, Switzerland.* Dr. Webb received his B.Sc, M.Sc, and Ph.D. degrees, all from the University of Manchester, in 1972, 1973, and 1975, respectively. After postdoctoral work at the IBM Thomas J. Watson Research Center in the area of electron-beam lithography, he has been involved in various aspects of micro-electronic device fabrication, including work on Josephson devices and gallium arsenide MESFETs. Dr. Webb is currently working on mirror-coating technology for semiconductor lasers.

Peter Wolf *IBM Research Division, Zurich Research Laboratory, Säumerstrasse 4, 8803 Rüschlikon, Switzerland.* Dr. Wolf studied physics and received a B.S. degree from the University of Karlsruhe in 1953, an M.S. degree from the University of Darmstadt in 1958, and a Ph.D. degree from the University of Mainz in 1963. In 1959, he joined the IBM Research Laboratory in Zurich, where he has worked on the spin dynamics of thin magnetic films, the dynamics of spin structures in rare-earth metals, microwave Schottky-barrier field-effect transistors (MESFETs), and applications of Josephson junctions in memories and high-speed samplers. At present, he is manager of a devices group, and since 1984 has been engaged in optoelectronic applications of III–V devices. Dr. Wolf is a member of the German Physical Society.